Solar Physics (2005) 231: 29–44

SPATIAL DISTRIBUTION AND NORTH–SOUTH ASYMMETRY OF CORONAL BRIGHT POINTS FROM MID-1998 TO MID-1999

R. BRAJŠA
Hvar Observatory, Faculty of Geodesy, University of Zagreb, Kačićeva 26, HR-10000 Zagreb, Croatia
(e-mail: romanb@geof.hr)

H. WÖHL
Kiepenheuer-Institut für Sonnenphysik, Schöneckstr. 6, D-79104 Freiburg, Germany

B. VRŠNAK and V. RUŽDJAK
Hvar Observatory, Faculty of Geodesy, University of Zagreb, Kačićeva 26, HR-10000 Zagreb, Croatia

F. CLETTE and J.-F. HOCHEDEZ
Observatoire Royal de Belgique (ORB), Ave. Circulaire 3, B-1180 Bruxelles, Belgium

G. VERBANAC
Geophysical Institute, Faculty of Science, University of Zagreb, Horvatovac bb, HR-10000 Zagreb, Croatia

and

M. TEMMER
Institut für Physik, Institutsbereich Geophysik, Astrophysik und Meteorologie, Universitätsplatz 5, A-8010 Graz, Austria

(Received 31 May 2005; accepted 14 June 2005)

Abstract. Full-disc full-resolution (FDFR) solar images obtained with the Extreme Ultraviolet Imaging Telescope (EIT) on board the Solar and Heliospheric Observatory (SOHO) were used to analyse the centre-to-limb function and latitudinal distribution of coronal bright points. The results obtained with the interactive and the automatic method, as well as for three subtypes of coronal bright points for the time period 4 June 1998 to 22 May 1999 are presented and compared. An indication of a two-component latitudinal distribution of coronal bright points was found. The central latitude of coronal bright points traced with the interactive method lies between 10° and 20°. This is closer to the equator than the average latitude of sunspots in the same period. Possible implications for the interpretation of the solar differential rotation are discussed. In the appendix, possible differences between the two solar hemispheres are analysed. More coronal bright points were present in the southern solar hemisphere than in the northern one. This asymmetry is statistically significant for the interactive method and not for the automatic method. The visibility function is symmetrical around the central meridian.

1. Introduction

Various magnetic features can be used as tracers for the determination of the solar differential rotation (Stix, 2002 and references therein). The character of the

deduced differential rotation can be influenced by the lifetime and size of the used objects and the duration of tracing (e.g., Snodgrass, 1992). Large-scale and long-lived tracers show generally more rigid characteristics of rotation than the small-scale and short-lived ones (Stix, 2002). In addition, the latitudinal distribution of features (e.g., Martin and Harvey, 1979; Harvey-Angle, 1993; Sattarov *et al.*, 2002) and especially possible north–south asymmetry found in certain investigations (Wang and Sheeley, 1989; Pulkkinen *et al.*, 1999; Temmer, Veronig, and Hanslmeier, 2002), may also significantly influence the results of the rotation analysis. The space/time interplay, represented by the butterfly diagram (Vršnak *et al.*, 1992; Harvey-Angle, 1993; Mouradian and Soru-Escaut, 1994; Riehokainen, Urpo, and Valtaoja, 1998; Benevolenskaya, Kosovichev, and Scherrer, 2001; Gelfreikh *et al.*, 2002), is also very important, especially when variations of the solar rotation in time are analysed (e.g., Balthasar, Vázquez, and Wöhl, 1986; Brajša *et al.*, 1997). The mean latitude of activity is an important reference point in the studies of rotation velocity residuals and meridional motions (Howard and LaBonte, 1980; Howard, 1991). It shifts during the solar activity cycle and also for the same phase from cycle to cycle (Pulkkinen *et al.*, 1999).

This paper continues our investigation of the solar differential rotation and other large-scale flows determined by tracing coronal EUV bright points. The results on the solar differential rotation for the period 4 June 1998 to 22 May 1999 were presented by Brajša *et al.* (2002). Properties of the solar velocity field indicated by motions of coronal bright points were analysed by Vršnak *et al.* (2003). This velocity field is described by the rotation velocity residual and the meridional motion, and their relationship is expressed through the horizontal Reynolds stress. Gissot *et al.* (2003) applied an optical flow method to pairs of successive EIT images of May 5, 1998. Depending on the latitude range, they found faster and slower rotational motions than the average qualitatively consistent with the result of Vršnak *et al.* (2003). A method of the simultaneous determination of the true solar synodic rotation velocity and the height of tracers was applied to the same data set (Brajša *et al.*, 2004).

In this paper, we analyse statistical properties of coronal bright points which might help to resolve some of the open questions left in previous studies. In particular we study the centre-to-limb function, the latitudinal distribution, and the north–south and west–east asymmetry of coronal bright points. The results for different methods (interactive and automatic) and tracer subtypes are presented and compared mutually, as well as with other data. Possible implications of these results on the analysis of the solar differential rotation, determined with the same data set (Brajša *et al.*, 2002), are discussed. In that paper we reported about a small rotational asymmetry indicating a somewhat faster rotation velocity in the northern solar hemisphere and here we extend the analysis also to the north–south latitudinal distribution.

The latitudinal distribution is especially interesting since coronal bright points are widely distributed over heliographic latitudes. This is often not the case for

typical tracers used for the solar rotation determination, which usually cover only lower and/or middle latitudes and it is important to extend the solar rotational analysis to higher latitudes (e.g., Fisk, 1996).

The spatial distributions are here presented separately for the two solar hemispheres, as well as for both of them together. The distributions for both solar hemispheres treated together were presented in a preliminary form by Brajša *et al.* (2003) where the differences between the three tracers subtypes were also discussed.

2. The Data Set and Methods of Data Reduction

The data set consists of 463 full-disc solar filtergrams recorded in the Fe XV line at the wavelength of 28.4 nm with the EIT instrument (Delaboudinière *et al.*, 1995) on board the SOHO spacecraft. Usually images were taken every 6 h, i.e., with a regular cadence of four images per day, although sometimes there were gaps of 12 h or more between the successive images. Measurements performed in June, November, and December 1998 and in March, April, and May 1999 are used here.

The interactive and the automatic methods of data reduction were introduced by Brajša *et al.* (2001). Using the interactive method, coronal bright points are visually traced in consecutive images on a computer screen. For the whole observing period, 4 June 1998 to 22 May 1999, two data sets reduced with the interactive method were established (Brajša *et al.*, 2002). In case of the "data set 1" the tracing was performed in up to 11 consecutive images and in case of the "data set 2" the tracing was performed in up to 24 consecutive images. In the case of the interactive method (and not for the automatic one) it is possible to distinguish between three different tracer subtypes, point-like structures (PLS), small loops (SL), and small active regions (SAR). In Brajša *et al.* (2002), the solar rotation was compared for the two methods, for the three tracer subtypes, and for the northern and the southern solar hemispheres.

The automatic method of data reduction is based on the Interactive Data Language (IDL) procedure "Regions Of Interest (ROI) segmentation". It is described in detail in Brajša *et al.* (2001, 2002). The ROI procedure was applied on triplets of images taken every 6 h. The numerical ROI parameters of the automatic method were chosen in such a way to resemble the interactive method as much as possible; the parameters which were used in the actual analysis were given in Brajša *et al.* (2002).

3. Results and Comparisons

In the differential rotation analysis the exclusion of the extreme rotation velocities was performed by the two-step velocity filter (Brajša *et al.*, 2001, 2002). However, in histograms in the present paper all data without the velocity filter are analysed,

since we are interested in spatial and temporal distributions of all identified coronal bright points. The analysis was also repeated applying the two-step velocity filter and no significant difference was found.

3.1. CENTRE-TO-LIMB FUNCTION OF CORONAL BRIGHT POINTS

In Figure 1, the west–east distributions of coronal bright points are presented for the interactive and automatic methods. The central meridian distance (CMD) is calculated as the mean value during the tracing for each identified bright point. In case of the interactive method, the CMD values were recorded for the data set 1 only. Positive and negative CMD values are treated separately and the sum of the graph is 100% for each hemisphere.

CMD distributions of coronal bright points, for both solar hemispheres taken together, are compared for the interactive (data set 1) and for the automatic method in Figure 2. The number of tracers in each longitude range can be obtained as the percentage multiplied by the total number n for each distribution given in the legend and in Table I (in the appendix). The same holds also for other histograms presented in this paper. For the interactive method a gradual decrease from the central meridian up to 90° is observed. The main differences between the interactive and the automatic methods are at CMD values less than 40°; the fraction of tracers for the automatic method firstly increases from 15.6% at central meridian regions to 18.8% at CMD values between 20° and 30° and then gradually decreases for larger CMD.

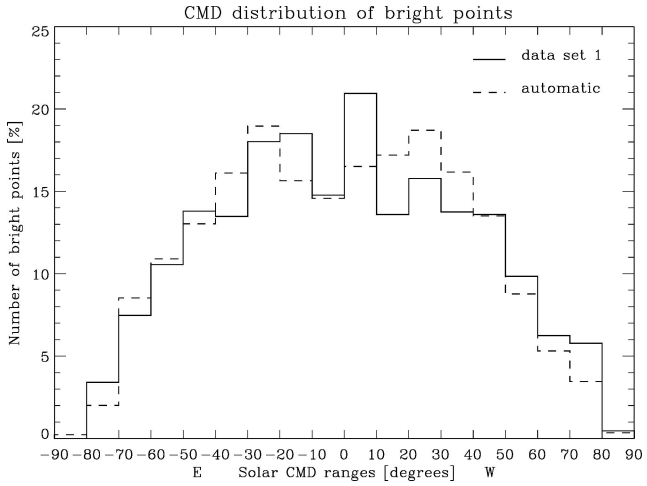

Figure 1. Central meridian distance (CMD) distribution of coronal bright points (interactive method, data set 1 and automatic method, see the legend). The eastern (western) solar hemisphere is represented by negative (positive) CMD values. Numbers of tracers for both hemispheres separately are given in Table I (in the appendix). Percentages on the y-axis refer to these numbers.

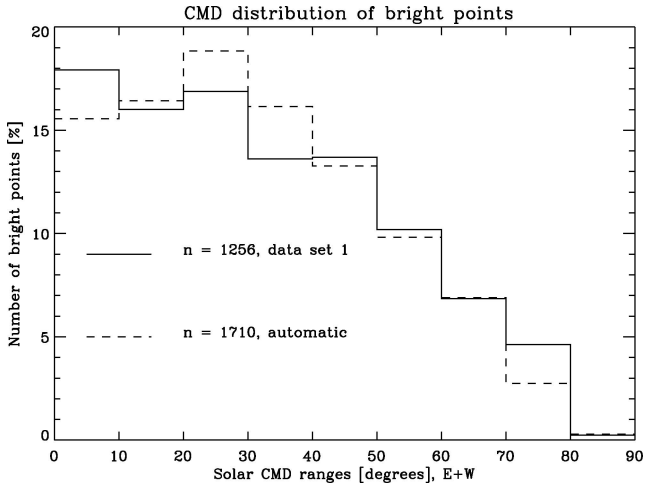

Figure 2. CMD distribution of coronal bright points for the interactive method (data set 1, *full line*) and for the automatic method (*dashed line*). Similar as in Figure 1, but here presented for the eastern and western solar hemispheres taken together.

The gradual decrease from the central meridian for the interactive method is similar to the CMD distribution of ephemeral regions (Harvey-Angle, 1993). On the other hand, the maximum for the automatic method is not at the central meridian, but between 20° and 30° of the CMD, similar to the CMD distribution of microwave low temperature regions (Vršnak *et al.*, 1992), where the maximum lies between 10° and 20° of the CMD and the number of observed low temperature regions decreases for lower and higher CMD values, as in the present case. This behaviour indicates that the discernability of tracers depends on the angle at which it is observed (the visibility function).

3.2. LATITUDINAL DISTRIBUTION OF CORONAL BRIGHT POINTS

In Figure 3, the north–south latitudinal distribution of coronal bright points is presented for the interactive method (data sets 1 and 2) and for the automatic method. The latitude of each bright point is represented as the mean value during the tracing.

The latitudinal distributions of coronal bright points, for both solar hemispheres taken together, are compared for the interactive (data sets 1 and 2) and for the automatic method in Figure 4. The number of tracers in each latitude range can be obtained as the percentage multiplied by the total number n for each distribution given in the legend and in Table II (in the appendix).

All three distributions presented in Figure 4 are similar in the sense that they have the maximum at latitudes between 10° and 20°. However, the main difference between the interactive and automatic method is at middle latitudes; the maximum

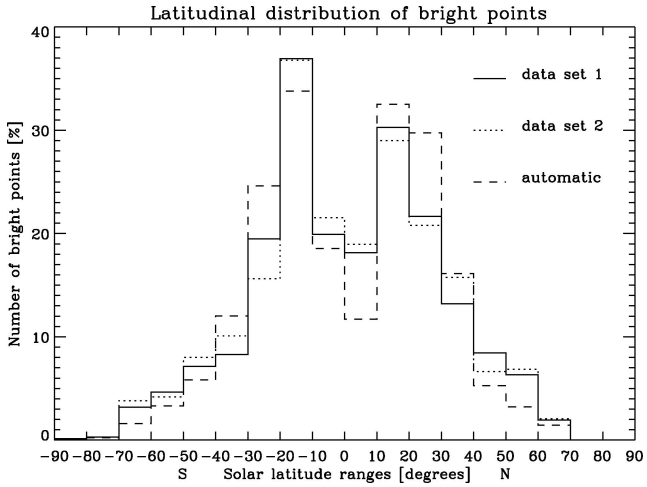

Figure 3. Latitudinal distribution of coronal bright points for the interactive method, data sets 1 and 2, and for the automatic method (see the legend). The northern (southern) solar hemisphere is represented by positive (negative) latitudes. Number of tracers for both hemispheres separately are given in Table II (in the appendix). Percentages on the *y*-axis refer to these numbers.

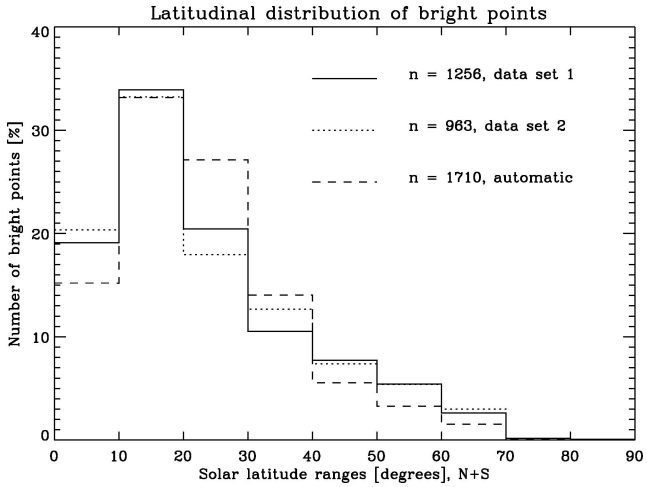

Figure 4. Latitudinal distribution of coronal bright points for the interactive method (data sets 1 and 2, *full* and *dotted line*, respectively) and for the automatic method (*dashed line*). Similar as in Figure 3, here presented for the northern and southern solar hemispheres taken together.

is broader and extended to 30° for the automatic method. We compare now the fractions of tracers at latitudes between 10° and 40° for the two methods. In case of the interactive method in this latitude range less than two-third of tracers were observed (64.9 and 63.9% for the data sets 1 and 2, respectively), while for the automatic method it was almost three-fourth (74.3%).

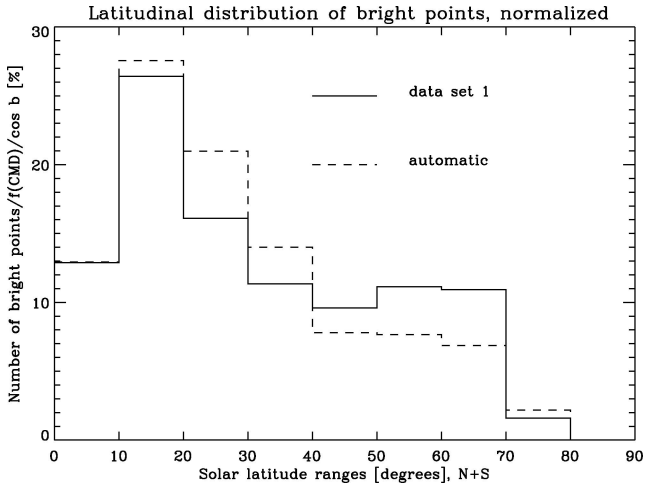

Figure 5. Similar as in Figure 4, here normalized with the factor $(\cos b)^{-1}$, where b is the latitude, and with the centre-to-limb function (Figure 2); for details see text.

To take into account smaller areas of equidistant latitude bands at medium and high latitudes and the centre-to-limb function of coronal bright points, we normalize the histogram in Figure 4 using a modified procedure developed by Harvey-Angle (1993) for bipolar active regions. First, the number of bright points in 10° latitude bins are multiplied by the factor $(\cos b)^{-1}$, where b is the latitude of the bin centre. Second, from the data presented in Figure 2, the centre to limb function f_{CMD}, normalized to have the value 1.0 at the maximum of each distribution, is calculated. Now the number of bright points in 10° latitude bins are multiplied by the factor f_{CMD}^{-1}. The histograms for the interactive and the automatic methods normalized with both factors are presented in Figure 5.

3.3. Comparison of the spatial distributions for different tracer subtypes

The CMD distributions for the three tracer subtypes indicate some differences which become less pronounced when the eastern and western solar hemispheres are folded together (Brajša *et al.*, 2003).

The latitudinal distribution (both solar hemispheres taken together) for various tracer subtypes identified with the interactive method is discussed in detail in Brajša *et al.* (2003). All three distributions for both data sets 1 and 2 have the maximum at latitudes between 10° and 20°. This maximum is highest (largest percent) for SARs and partly extended to 30°. So, the latitudinal distribution for the SAR subsample is most similar to the one obtained with the automatic method. The latitudinal distributions for the other two tracer subsamples, PLSs and SLs, are more uniform.

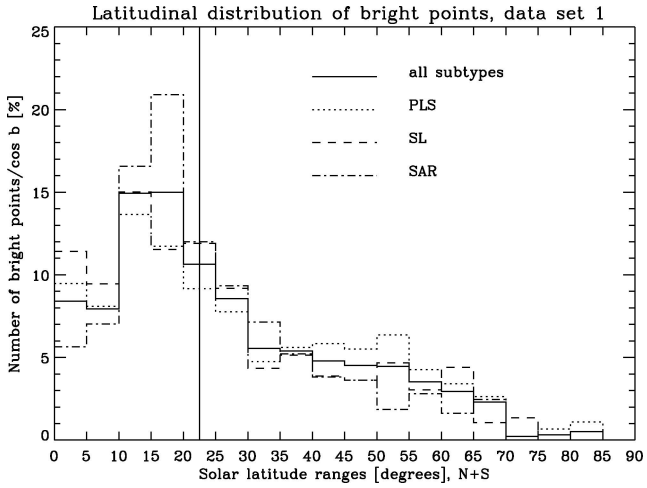

Figure 6. Latitudinal distribution of coronal bright points for the interactive method (data set 1), presented also for the three tracer subtypes, as indicated in the legend. Similar as in Figure 4 (*full line*), here presented for 5° latitude bins and normalized with the factor $(\cos b)^{-1}$, where b is the latitude. The vertical full line denotes the mean latitude of sunspots in the observing period.

To study the latitudinal distribution for various tracer subtypes in more detail, we now present in Figure 6 the latitudinal distribution of coronal bright points (interactive method, data set 1) for 5° latitude bins, as an example. Here, only the normalization with the factor $(\cos b)^{-1}$ is applied. It is interesting to note that the maxima for PLSs and SARs do not coincide in latitude: for PLSs the maximum is in the range 10°–15° and for SARs in the range 15°–20°. Furthermore, the distribution of PLSs is smoother over latitudes in comparison with the SARs. This finding is consistent with the observations of magnetic ephemeral regions, which indicate that the distribution of ephemeral regions becomes more uniform as their size decreases (Harvey-Angle, 1993; Hagenaar, Schrijver, and Title, 2003). We would like to note that the different behaviour of magnetic regions with fluxes below and above $\approx 30 \times 10^{18}$ Mx has led Hagenaar, Schrijver, and Title (2003) to propose that smaller magnetic regions have their origin in a turbulent, small-scale dynamo, mostly independent of the global solar cycle.

We calculate now the mean latitude of all coronal bright points in two ways, as a simple mean and applying statistical weights to take into account that different tracer subtypes have different sizes

$$\xi_0 = \frac{\sum b_i}{n}, \quad \xi_0^{\mathrm{SW}} = \frac{\sum b_i \mathrm{SW}_i}{\sum \mathrm{SW}_i}, \tag{1}$$

where b_i represents the latitude of the ith bright point, SW_i its statistical weight according to the area, and n is the total number of them. We take $\mathrm{SW} = 1$ for PLSs,

SW = 3 for SLs, and SW = 11 for SARs according to typical areas of the three tracer subtypes, normalized to the average area of PLSs (Brajša *et al.*, 2002). For the interactive method, data set 1 we obtain $\xi_0 = 22.98^\circ$ and $\xi_0^{\mathrm{SW}} = 22.19^\circ$. Both values lie very close to the mean latitude of sunspots in the same period, which was placed at about 22.5° (see Figure 6).

Let us make here a comment on the terminology. The *mean latitude* of tracers is calculated according to either of the Equation (1), while the *central latitude* of tracers corresponds to the latitudinal position of the highest peak in the distribution (modus). The two latitudes do not necessarily coincide, as can be seen by comparing ξ_0 and ξ_0^{SW} with the distribution presented in Figure 6. This difference is caused by the asymmetry of the distribution.

4. Discussion and Conclusion

4.1. Latitudinal distribution and north–south asymmetry of coronal bright points

The maximum in the latitudinal distribution of coronal bright points for both solar hemispheres and all three tracer subtypes taken together is between 10° and 20° (interactive method, Figures 4–6). This is closer to the equator than the mean latitude of sunspots for the same time period which was located at about 22.5° (Figure 6). Some structures in the solar atmosphere dominantly populate latitudes shifted from the centres of sunspot activity, e.g., low brightness temperature regions observed in microwaves (Vršnak *et al.*, 1992; Gelfreikh *et al.*, 2002). Depending on the solar cycle phase, 39–76% of these regions were associated with Hα filaments (Brajša *et al.*, 1999) which significantly populate latitudes also outside the sunspot belts.

Next we discuss the distribution of coronal bright points for 10° latitude bins, both solar hemispheres taken together, normalized by the factors $(\cos b)^{-1}$ and f_{CMD}^{-1} (Figure 5). The histogram indicates a possibility of a two-component distribution. The first one is uniformly distributed from the equator up to the latitude of 70° and the other one is superimposed on it, having the maximum at the latitudes 10°–20° for the interactive method and at the latitudes 10°–30° for the automatic method. The two-component latitudinal distribution of coronal bright points was introduced by Golub, Krieger, and Vaiana (1975) who analysed the Skylab data. However, these authors have found that the second distribution was mostly confined to the regions from the equator up to the latitude of 30° (Golub, Krieger, and Vaiana, 1975), while we found no signature of the second distribution at equatorial regions. This difference can be attributed to the different solar cycle phases when the measurements were performed: in 1973, before the minimum (Skylab data) and in 1998–1999, before the maximum (present work), but also to different wavelength ranges used. This is also consistent with the latitudinal distributions of coronal

bright points observed in soft X-rays with the Yohkoh spacecraft during different years (Sattarov *et al.*, 2002).

Finally we discuss the north–south latitudinal asymmetry of coronal bright points (Figure 3 and Table II in the appendix). Sattarov *et al.* (2002) presented the yearly latitudinal distributions of coronal bright points observed in soft X-rays with the Yohkoh spacecraft. Their distributions for the years 1998 and 1999 (Figure 2 in Sattarov *et al.*, 2002), embracing our period of analysis, are generally similar in shape to our distributions. In our data set, more coronal bright points were found in the southern solar hemisphere than in the northern one. This asymmetry is statistically significant for the interactive method and not for the automatic method. We stress that this north–south asymmetry refers only to a relatively short time span of observations, i.e., the period 4 June 1998 to 22 May 1999.

We note that the higher population of bipolar magnetic regions in the northern hemisphere in the same activity phase (as our measurements) was found two solar cycles earlier (Wang and Sheeley, 1989; based on an analysis of 2700 bipolar magnetic regions during 1976–1986). In the same time period a similar result was found for the ephemeral regions (Harvey-Angle, 1993; there are 100–150 ephemeral regions at any given time in the rising phase of the solar activity). Furthermore, the rising phase of the solar cycle 23 (including our period of measurements) is characterized with a slight excess of the cumulative monthly mean Sunspot Numbers in the northern hemisphere (Temmer, Veronig, and Hanslmeier, 2002). In the period mid-1998 to mid-1999, there was also a distinct north–south asymmetry of the number of Hα flares in favour of the northern hemisphere (Temmer *et al.*, 2001, their Figure 9; based on an analysis of almost 100 000 events occurred during 1975–1999).

All this is consistent with the assumption that the visibility of coronal bright points might be influenced by the background coronal brightness affected by the presence of active regions (Sattarov *et al.*, 2002 and references therein). So, when many active regions are present in a solar hemisphere, the possibility to observe coronal bright points is smaller, and vice versa. This is consistent with the mentioned two-component distribution, which is most prominent in the saddle-type distribution of PLSs around middle solar latitudes (Figure 6). A similar situation was found with the microwave low brightness temperature regions which can hardly be observed in the vicinity of ordinary sunspot active regions because of high emission at these places (Vršnak *et al.*, 1992; Brajša *et al.*, 1994).

To interpret the north–south asymmetry in solar activity, Ossendrijver, Hoyng, and Schmidt (1996) have shown that stochastic fluctuations of the parameter α in a mean field dynamo model can reproduce the observed asymmetries. Observational and theoretical issues concerning the north–south asymmetry of the solar activity were recently reviewed by Ossendrijver (2003) and Rüdiger and Hollerbach (2004). We note also that pronounced indications for a cycle-dependence of the north–south asymmetry were reported (Verma, 1993; Joshi, 1995; see also Ballester, Oliver, and Carbonell, 2005).

4.2. Implications for the interpretation of the solar differential rotation

Solar rotation determined with the automatic method was found to be less differential in comparison with the interactive method (Brajša *et al.*, 2002). To explain this rigid rotation component deduced with the automatic method in Brajša *et al.* (2002) we proposed the possibility that in some cases parts of large active regions were identified and traced with the automatic method. This possibility is consistent with the latitudinal distributions of coronal bright points presented in this paper. Almost three-fourth of all coronal bright points were identified in active region belts, at latitudes between 10° and 40°, with the automatic method. The corresponding fraction was less than two-third for the interactive method. As discussed in Brajša *et al.* (2002), with the interactive method only isolated structures on smaller scales were identified, since larger structures can be excluded by visual inspection.

The similarities in rotation velocity and latitudinal distributions between the SAR subsample of the interactive method and the automatic method sample are also in agreement with the above mentioned hypothesis. We can consider SARs as tracers on the medium scale, between PLSs and SLs on smaller scales and ordinary active regions on the larger scales.

In Brajša *et al.* (2002), we reported about a small rotational asymmetry indicating a somewhat faster rotation velocity in the northern solar hemisphere at medium and high latitudes (data set 1 of the interactive method and automatic method). The profile of the solar rotation is less differential in the north than in the south, the difference of the parameter B being statistically significant above and below the 1σ level for the two methods mentioned, respectively. The observed north–south asymmetry of the solar differential rotation could perhaps be interpreted by the interaction between differential rotation and magnetic fields. Recently, Brun (2004) described how Maxwell stresses oppose Reynolds stresses and in this way can transport angular momentum towards solar poles, reducing the differential rotation. Brun (2004) described how a reduced level of magnetism in the solar convection zone could have lead to a more pronounced differential rotation during the Maunder minimum, for which there are some observational indications. We can here extend this line of reasoning and put forward the following hypothesis: the northern solar hemisphere was magnetically more active during the period of our observations (Section 4.1) leading to a less differential rotation profile for the northern hemisphere, as observed by Brajša *et al.* (2002).

Acknowledgements

This work was performed with the support of the Alexander von Humboldt Foundation and is related to the SOHO-EIT Proposal Brajsa_206: 'An analysis of the solar rotation velocity by tracing coronal features' (http://umbra.nascom.

nasa.gov/eit/proposals/) submitted in March 1999 by R. Brajša, B. Vršnak, V. Ruždjak, D. Roša, H. Wöhl, and F. Clette. SOHO is a project of international cooperation between ESA and NASA. We would like to thank the EIT team for developing and operating the instrument, and J. Bruls and A. Nesis for helpful discussions. F. Clette and J.-F. Hochedez acknowledge the support from the Belgian Federal Science Policy Office through the ESA-PRODEX programme. M. Temmer gratefully acknowledges financial support by the Austrian Science Fund (FWF project P15344).

Appendix: An Estimate of the Possible North–South and West–East Distribution Asymmetry

The north–south asymmetry of the solar activity was investigated using sunspots (e.g., Carbonell, Oliver, and Ballester, 1993; Oliver and Ballester, 1994; Pulkkinen *et al.*, 1999; Temmer, Veronig, and Hanslmeier, 2002) and other solar activity phenomena, such as flares observed in different wavelength ranges, prominences, radio bursts, and green coronal brightness (e.g., Özgüc and Ücer, 1987; Verma, 1993; Joshi, 1995; Temmer *et al.*, 2001; Joshi and Pant, 2005). Further, the west–east asymmetry of various manifestations of solar activity was analysed by Letfus (1960), Dezső (1964), Joshi (1995), and Joshi and Pant (2005). The asymmetry A_{NS} of the north–south distribution and the asymmetry A_{WE} of the west–east distribution are calculated according to

$$A_{\mathrm{NS}} = \frac{N - S}{N + S}, \quad A_{\mathrm{WE}} = \frac{W - E}{W + E}. \tag{2}$$

where N, S, W, and E are the numbers of coronal bright points identified in the northern, southern, western, and eastern solar hemispheres, respectively.

To estimate the statistical significance of the north–south asymmetry of any objects in the solar atmosphere we inspect the probability of the deduced distribution. In general, the probability of the outcome r out of the n trials can be calculated using the binomial distribution

$$P(r) = \frac{n!}{r!(n-r)!} p^r (1-p)^{n-r}. \tag{3}$$

where p is the probability of the class in question (e.g., Feynman, Leighton, and Sands, 1963; Anderson and Finn, 1996). In particular, when $p = 0.5$, as in our case, the above equation reduces to

$$P(r) = \frac{n!}{r!(n-r)!} 2^{-n}. \tag{4}$$

We now calculate the sum of probabilities in the binomial distribution from a given point r to the end of the distribution and double it, since both tails are

symmetric

$$P = 2\sum_{i=r}^{n} P(i), \tag{5}$$

We take always $r \geq n/2$.

When $P > 10\%$ the asymmetry is statistically not significant, for $5\% < P < 10\%$ it is marginally significant, when $1\% < P < 5\%$ the result is statistically significant, and for $P < 1\%$ it is highly significant (Carbonell, Oliver, and Ballester, 1993; Oliver and Ballester, 1994). The statistical significance of the possible west–east asymmetry can be estimated in an analogous way.

In Table I, the number of coronal bright points traced in the eastern and the western solar hemisphere is expressed in percents for the two methods of data reduction and for different tracer subtypes. The west–east asymmetry A_{WE} and the probability P were calculated according to Equations (2) and (5), respectively. It can be seen that in all cases the west–east asymmetry is not statistically significant implying the symmetric visibility of coronal bright points.

In Table II, the number of coronal bright points traced in the northern and the southern solar hemisphere is presented for the interactive method (data sets 1 and 2, for all data and for different tracer subtypes) and for the automatic method. The asymmetry of the north–south distribution A_{NS} is calculated according to Equation (2) and the probability P according to Equation (5). In all cases more coronal bright points were found in the southern solar hemispheres, than in the northern one, so that $r = S$ was used (Table II).

TABLE I

The west–east CMD distribution of coronal bright points for the interactive (data set 1, INT1) and the automatic (AUT) methods.

	All	PLS	SL	SAR	Method
W	640 (51.0%)	292 (50.5%)	115 (54.5%)	233 (49.9%)	INT1
E	616 (49.0%)	286 (49.5%)	96 (45.5%)	234 (50.1%)	INT1
n	1256	578	211	467	INT1
A_{WE}	+0.019	+0.010	+0.090	−0.002	INT1
P	51.6%	83.5%	21.5%	100.0%	INT1
W	866 (50.6%)				AUT
E	844 (49.4%)				AUT
n	1710				AUT
A_{WE}	+0.013				AUT
P	61.2%				AUT

Note. PLS: point-like structure; SL: small loop; SAR: small active region; W: the number of tracers in the western hemisphere; E: the number of tracers in the eastern hemisphere; n: the total number of tracers; A_{WE}: the W–E asymmetry; P: the probability.

TABLE II

The north–south latitudinal distribution of coronal bright points for the interactive (data sets 1 and 2, INT1 and INT2, respectively) and the automatic (AUT) methods.

	All	PLS	SL	SAR	Method
N	568 (45.2%)	237 (41.0%)	102 (48.3%)	229 (49.0%)	INT1
S	688 (54.8%)	341 (59.0%)	109 (51.7%)	238 (51.0%)	INT1
n	1256	578	211	467	INT1
A_{NS}	−0.096	−0.180	−0.033	−0.019	INT1
P	0.078%	0.002%	68.0%	71.1%	INT1
N	438 (45.5%)	170 (46.4%)	114 (45.6%)	154 (44.4%)	INT2
S	525 (54.5%)	196 (53.6%)	136 (54.4%)	193 (55.6%)	INT2
n	963	366	250	347	INT2
A_{NS}	−0.090	−0.071	−0.088	−0.112	INT2
P	0.56%	19.1%	18.4%	4.1%	INT2
N	837 (48.9%)				AUT
S	873 (51.1%)				AUT
n	1710				AUT
A_{NS}	−0.021				AUT
P	39.7%				AUT

Note. PLS: point-like structure; SL: small loop; SAR: small active region; N: the number of tracers in the northern hemisphere; S: the number of tracers in the southern hemisphere; n: the total number of tracers; A_{NS}: the N–S asymmetry; P: the probability.

From Table II, we can see that we have a highly significant difference for the interactive method (both data sets, all tracer subtypes taken together) and a nonsignificant difference for the automatic method. When tracer subtypes are considered separately, a highly significant result was obtained for the PLSs and a nonsignificant result for the other two tracer subtypes (data set 1). For the data set 2, we have a non-significant difference for PLSs and SLs and a statistically just significant result for SARs.

References

Anderson, T. W. and Finn, J. D.: 1996, *The New Statistical Analysis of Data*, Springer-Verlag, New York.

Ballester, J. L., Oliver, R., and Carbonell, M.: 2005, *Astron. Astrophys.* **431**, L5.

Balthasar, H., Vázquez, M., and Wöhl, H.: 1986, *Astron. Astrophys.* **155**, 87.

Benevolenskaya, E. E., Kosovichev, A. G., and Scherrer, P. H.: 2001, *Astrophys. J.* **554**, L107.

Brajša, R., Pohjolainen, S., Ruždjak, V., Teräsranta, H., Urpo, S., Vršnak, B., and Wöhl, H.: 1994, in M. Schüssler and W. Schmidt (eds.), *Solar Magnetic Fields*, Proceedings of International Conference held in Freiburg, Cambridge University Press, Cambridge, p. 62.

Brajša, R., Ruždjak, V., Vršnak, B., Pohjolainen, S., Urpo, S., Scholl, A., and Wöhl, H.: 1997, *Solar Phys.* **171**, 1.

Brajša, R., Ruždjak, V., Vršnak, B., Wöhl, H., Pohjolainen, S., and Urpo, S.: 1999, *Solar Phys.* **184**, 281.

Brajša, R., Wöhl, H., Vršnak, B., Ruždjak, V., Clette, F., and Hochedez, J. F.: 2001, *Astron. Astrophys.* **374**, 309.

Brajša, R., Wöhl, H., Vršnak, B., Ruždjak, V., Clette, F., and Hochedez, J. F.: 2002, *Astron. Astrophys.* **392**, 329.

Brajša, R., Wöhl, H., Vršnak, B., Ruždjak, V., Clette, F., Hochedez, J. F., Roša, D., and Hržina, D.: 2003, *Hvar Observ. Bull.* **27**, 13.

Brajša, R., Wöhl, H., Vršnak, B., Ruždjak, V., Clette, F., Hochedez, J. F., and Roša, D.: 2004, *Astron. Astrophys.* **414**, 707.

Brun, A. S.: 2004, *Solar Phys.* **220**, 333.

Carbonell, M., Oliver, R., and Ballester, J. L.: 1993, *Astron. Astrophys.* **274**, 497.

Delaboudinière, J. P., Artzner, G. E., Brunaud, J., Gabriel, A. H., Hochedez, J. F., Millier, F., *et al.*: 1995, *Solar Phys.* **162**, 291.

Dezső, L.: 1964, *Third Consultation on Solar Physics and Hydrodynamics, Czechosl. Acad. Sci. Astron. Inst. Pub.* **51**, 49.

Feynman, R. P., Leighton, R. B., and Sands, M.: 1963, *The Feynman Lectures on Physics* I, vol. I, chapter 6, Addison-Wesley, Reading, MA.

Fisk, L. A.: 1996, *J. Geophys. Res.* **101**, 15547.

Gelfreikh, G. B., Makarov, V. I., Tlatov, A. G., Riehokainen, A., and Shibasaki, K.: 2002, *Astron. Astrophys.* **389**, 618.

Gissot, S. F., Hochedez, J.-F., Dibos, F., Brajša, R., Jacques, L., Berghmans, D., Zhukov, A., Clette, F., Wöhl, H., and Antoine, J.-P.: 2003, in *Solar Variability as an Input to the Earth's Environment*, Proceedings of ISCS 2003 Symposium, ESA **SP-535**, p. 853.

Golub, L., Krieger, A. S., and Vaiana, G. S.: 1975, *Solar Phys.* **42**, 131.

Hagenaar, H. J., Schrijver, C. J., and Title, A. M.: 2003, *Astrophys. J.* **584**, 1107.

Harvey-Angle, K. L.: 1993, *Magnetic Bipoles on the Sun*, Ph.D. thesis, University of Utrecht, Utrecht.

Howard, R. F.: 1991, *Solar Phys.* **135**, 327.

Howard, R. and LaBonte, B. J.: 1980, *Astrophys. J.* **239**, L33.

Joshi, A.: 1995, *Solar Phys.* **157**, 315.

Joshi, B. and Pant, P.: 2005, *Astron. Astrophys.* **431**, 359.

Leftus, V.: 1960, *Publ. Astron. Inst. Czechosl.* **11**, 31.

Martin, S. F. and Harvey, K. L.: 1979, *Solar Phys.* **64**, 93.

Mouradian, Z. and Soru-Escaut, I.: 1994, *Astron. Astrophys.* **290**, 279.

Oliver, R. and Ballester, J. L.: 1994, *Solar Phys.* **152**, 481.

Ossendrijver, M., Hoyng, P., and Schmitt, D.: 1996, *Astron. Astrophys.* **313**, 938.

Ossendrijver, M.: 2003, *Astron. Astrophys. Rev.* **11**, 287.

Özgüc, A. and Ücer, C.: 1987, *Solar Phys.* **114**, 141.

Pulkkinen, P. J., Brooke, J., Pelt, J., and Tuominen, I.: 1999, *Astron. Astrophys.* **341**, L43.

Riehokainen, A., Urpo, S., and Valtaoja, E.: 1998, *Astron. Astrophys.* **333**, 741.

Rüdiger, G. and Hollerbach, R.: 2004, *The Magnetic Universe*, Wiley-VCH, Weinheim, p. 95.

Sattarov, I., Pevtsov, A. A., Hojaev, A. S., and Sherdonov, C. T.: 2002, *Astrophys. J.* **564**, 1042.

Snodgrass, H. B.: 1992, in K. L. Harvey (ed.), *The Solar Cycle*, Proceedings of the 12th Sacramento Peak Summer Workshop, ASP Conference Series, vol. 27, p. 71.

Stix, M.: 2002, *The Sun*, Springer-Verlag, Berlin, p. 277.

Temmer, M., Veronig, A., and Hanslmeier, A.: 2002, *Astron. Astrophys.* **390**, 707.

Temmer, M., Veronig, A., Hanslmeier, A., Otruba, W., and Messerotti, M.: 2001, *Astron. Astrophys.* **375**, 1049.
Verma, V. K.: 1993, *Astrophys. J.* **403**, 797.
Vršnak, B., Pohjolainen, S., Urpo, S., Teräsranta, H., Brajša, R., Ruždjak, V., Mouradian, Z., and Jurač, S.: 1992, *Solar Phys.* **137**, 67.
Vršnak, B., Brajša, R., Wöhl, H., Ruždjak, V., Clette, F., and Hochedez, J. F.: 2003, *Astron. Astrophys.* **404**, 1117.
Wang, Y.-M. and Sheeley, N. R., Jr.: 1989, *Solar Phys.* **124**, 81.